How to cite: *Angew. Chem. Int. Ed.* **2022,** *61,* e202205803
International Edition: doi.org/10.1002/anie.202205803
German Edition: doi.org/10.1002/ange.202205803

Photochemistry

Ultrafast Dynamics of Photochemical Nitrile Imine Formation

*Stefan Flesch and Peter Vöhringer**

Dedicated to Rudolph Clausius (1822–1888) on the occasion of his 200th birthday

Abstract: The chemical reactivity of nitrile imines is of great utility in organic synthesis with applications rapidly expanding into the materials and life sciences. Yet, our understanding of the electronic and molecular structures of nitrile imines remains incomplete and the elementary mechanism of their photoinduced generation is entirely unknown. Here, femtosecond infrared spectroscopy after 266 nm-excitation of 2,5-diphenyltetrazole has been carried out to temporally resolve the formation and structural relaxation dynamics of the nascent diphenylnitrile imine in liquid solution under ambient conditions. The infrared-spectroscopic evolution is interpreted by an initial sequence of intersystem crossings within 250 fs followed by the cleavage of N_2 with formation of a structurally relaxed nitrile imine on the adiabatic ground-state singlet surface within a few tens of picoseconds. The infrared spectrum supports the notion of a "floppy" nitrile imine molecule whose equilibrium character ranges from fully propargylic to fully allenic in the room temperature liquid solution.

Introduction

Nitrile imines are highly intriguing reactive intermediates in organic synthesis;[1] particularly, in 1,3-dipolar cycloaddition reactions[2] with applications in the construction of five-membered heterocycles and natural products,[3] polymer functionalization[4] and cross-linking,[5] cell-adhesive surface patterning,[6] as well as peptide and protein tagging.[7] Even in the absence of a substrate, nitrile imines are elusive species that rapidly decay and therefore need to be prepared in situ for a desired application. Matrix isolation techniques have enabled the unambiguous detection of such species[8] and when combined with high-resolution infrared (IR) spectroscopy and quantum chemical calculations, detailed information about their molecular structure and their chemical reactivity under cryogenic conditions can be obtained.[9]

The nitrile imine class of compounds presents a formidable challenge for electronic structure theory because a complete valence bond description requires no less than six distinct canonical structures as depicted in Figure 1a.[9b,10] Which of these six resonance forms dominate the valence-bond wave function depends critically on the nature of the substituents, R and R′. The simplest representative, formonitrile imine, H–CNN–H, adopts the axially chiral allenic structure, (ii), with the propargylic form, (i), constituting a transition state for the stereomutation of (ii).[10a,b,11]

Nitrile imines can be prepared either by dehydrochlorination of hydrazonyl halides or by dinitrogen elimination from 2,5-disubstituted tetrazoles.[1a] The latter reaction can be regarded as a retro-[3+2]-cycloaddition, or, more correctly, as a 1,3-dipolar cycloelimination of N_2 from the tetrazole.[10d,12] It is most often carried out photolytically (see Figure 1b and Supporting Information, Scheme S1), but to the best of our knowledge, the molecular-level mechanism of the N_2-extrusion from tetrazoles has not yet been explored in a time-resolved fashion. There exists only an early flash-photolysis study of tetrazoles by George and coworkers[13] but its time-resolution was limited to several

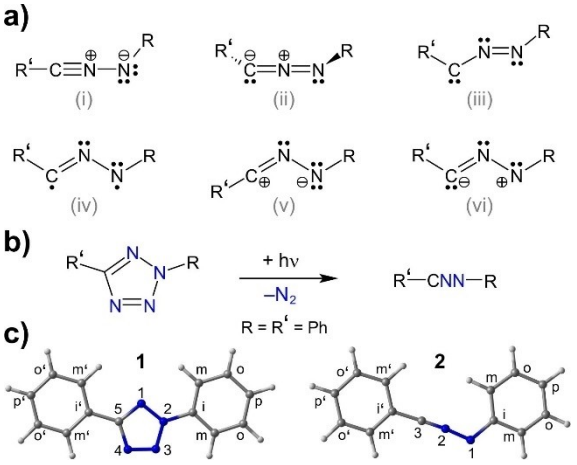

Figure 1. a) Six limiting valence isomers of nitrile imines: (i) propargylic, (ii) allenic, (iii) carbenic, (iv) diradical, (v) 1,3-dipolar (or allylic), and (vi) reverse 1,3-dipolar. b) Photolytic generation of nitrile imines from tetrazoles. c) DFT-optimized molecular structures with atom labels of diphenyltetrazole (**1**), and diphenylnitrile imine (**2**), (R = R′ = phenyl, Ph, cf. also structural data given in the Supporting Information).

[*] S. Flesch, Prof. Dr. P. Vöhringer
Clausius-Institut für Physikalische und Theoretische Chemie,
Rheinische Friedrich-Wilhelms-Universität
Wegelerstraße 12, 53115 Bonn (Germany)
E-mail: p.voehringer@uni-bonn.de

nanoseconds and the spectral kinetics were monitored in the ultraviolet-to-visible (UV/Vis) region; thus, details about the dynamic evolution of the molecular and electronic structure of the system following the initial photon absorption remained entirely hidden.

Here, we wish to fill this gap for the first time by studying the photochemistry of the model system, diphenyltetrazole **1** (cf. Figure 1c), in tetrahydrofuran (THF) solution under ambient conditions, following its photoexcitation with 50 fs duration laser pulses centered at 266 nm. Taking advantage of the unique structure-specificity of femtosecond infrared (IR) detection,[14] we set out to monitor directly in the time domain the formation and relaxation dynamics of a nitrile imine bearing a phenyl ring at each of the two terminal atoms of the central CNN-moiety (i.e. diphenylnitrile imine **2**, R = R′ = Ph). The analysis of the rich time-resolved spectra is facilitated here by accompanying electronic structure calculations based on density functional theory (DFT, see Supporting Information for experimental and computational methods.)

Results and Discussion

The electronic absorption spectrum of **1** in liquid THF solution is shown in Figure 2a. In the near UV, it consists of two broad bands peaking at 274 nm and 241 nm. The absorption profile is modulated by a pronounced Franck–Condon progression with a spectral spacing of roughly 920 cm^{-1} indicating that the S_1-state is bound. This interpretation is further corroborated by a measurement of the stationary fluorescence spectrum (cf. Figure 2a), which peaks at 319 nm corresponding to a peak-to-peak Stokes shift of roughly 5150 cm^{-1}. The total fluorescence quantum yield, Φ_f, was estimated to be no more than 4 % (see Figure S1 and Table S1). A fluorescence lifetime of 1.4 ns was determined by time-correlated single photon counting (cf. Figure S2).

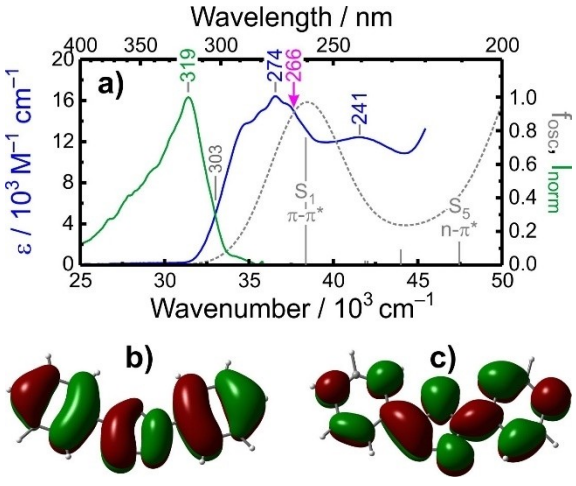

Figure 2. a) Experimental electronic absorption (solid blue) and emission (solid green) spectrum of **1** in THF-solution under ambient conditions and theoretical absorption spectrum based on TD-DFT calculations (dashed). Numbers indicate spectral position (in nm) of band maxima, 0-0-transition and excitation photon, respectively. b) and c) Highest occupied and lowest unoccupied transition orbital, respectively, corresponding to the $S_0 \rightarrow S_1$ transition. Difference electron densities are given in the Supporting Information.

According to quantum-chemical calculations based on time-dependent (TD) DFT, the 274 nm-band arises from the π–π* transition accessing the first excited singlet state, S_1, of the solute (cf. Figure 2b and c for the highest occupied and lowest unoccupied transition orbitals, respectively[15]). A geometry optimization of the S_1-state followed by a normal mode analysis confirms the bound nature of this lowest singlet π–π* state and suggests that the 920 cm^{-1}-progression results from an asymmetric in-plane deformation of the central tetrazole ring (cf. Figures S3 to S5 for optimized geometries and their DFT-predicted vibrational spectra). Note that the lowest singlet excited state of the simplest congener of **1**, 2*H*-tetrazole (R = R′ = H in Figure 1b), is a n–π*-state and not a π–π*-state as evidenced by complete active space self-consistent field and multireference configuration interaction methods.[16] The DFT-level-of-theory chosen here is able to reproduce this result fully (see Figure S6 for a detailed discussion of the electronic structure of **1** and its relation to that of 2*H*-tetrazole). However, according to the very same DFT-method, the lowest n-π*-state of **1** is actually S_5 and as such it is much higher in energy that the lowest π-π* state. It turns out that S_5 is also a bound state and when geometrically relaxed, it is located at an energy of ≈85.7 kJ mol^{-1} (or ≈7165 cm^{-1}) above the relaxed S_1 (see Table S2 for the energetics of the photochemistry and photophysics of **1**). It is therefore quite likely than the lowest n-π* state contributes to the absorption band at shorter wavelengths around 241 nm. The peculiar n–π*/π–π* state reversal upon introduction of the two phenyl rings results simply from the mixing of the π-orbitals on the central N-heterocycle with those on the peripheral aryls.

The Fourier-transform infrared (FTIR) spectrum of **1** in THF solution is displayed in Figure 3, top panel. The spectrum emphasizes the absorption bands arising from vibrational motions that are predominantly localized on either of the two phenyl rings, Ph and Ph′ (a_1-vibrational species in the local C_{2v}-symmetry of a monosubstituted benzene). Importantly, except for the phenyl CH-stretching modes around 3100 cm^{-1}, tetrazole, **1**, does not have any appreciable IR-activity for wavenumbers larger than 1640 cm^{-1} (cf. Figure S5).

According to the DFT-calculations, the pair of bands peaking at 1497 cm^{-1} and 1530 cm^{-1} originates from the ($\mathcal{M}_5$) and ($\mathcal{M}_5$)′-modes of the Ph and Ph′ substituents, respectively, whose character is primarily CH in-plane bending (see Figure 1c for atom labels. Mulliken numbering as recommended in Ref. [17] is used here; see inset Figures 3 as well as Figures S7 and S8 for atomic displacement vectors of these ring modes). In contrast, the two bands located at 1597 cm^{-1} and 1611 cm^{-1} are due to the ($\mathcal{M}_4$) and ($\mathcal{M}_4$)′-modes involving mostly symmetric C^oC^m and $C^{o'}C^{m'}$-stretching motion, which is coupled to CH-in-plane bending. In addition, the ($\mathcal{M}_4$) and ($\mathcal{M}_5$) modes also modulate the N^2C^i-distance whereas the ($\mathcal{M}_4$)′ and ($\mathcal{M}_5$)′ modes give rise to an

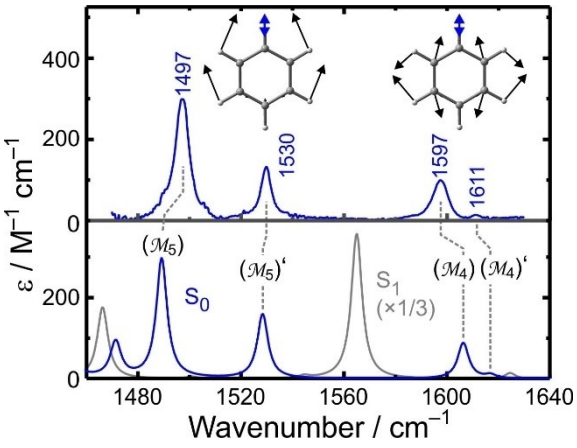

Figure 3. Experimental stationary FTIR spectrum of **1** in liquid THF (blue curve, upper panel) in comparison with a predicted spectrum of **1** derived from DFT (blue curve, lower panel). The gray spectrum is a DFT-predicted spectrum of **1** in its S_1-state and its intensity was divided by 3. The insets sketch the atomic displacements involved in the ($\mathcal{M}_4$) and ($\mathcal{M}_5$)-modes of the phenyl rings.

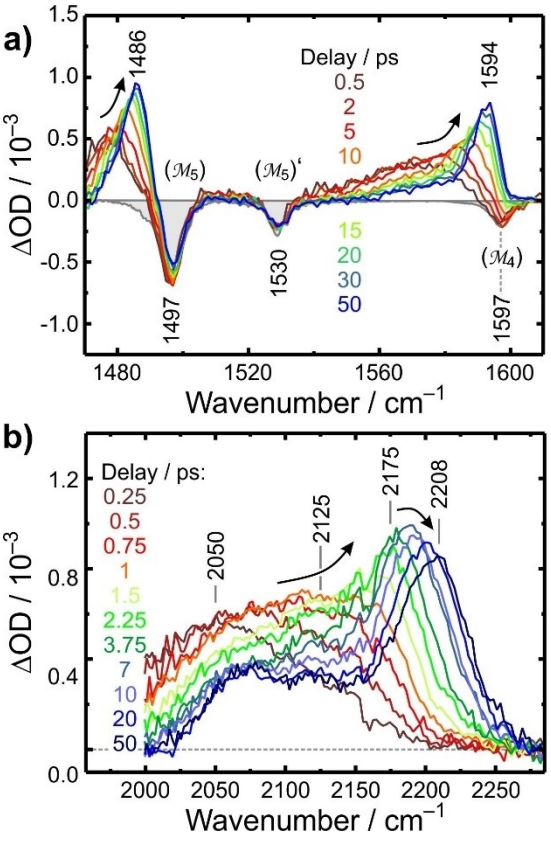

Figure 4. UV-pump/MIR-probe spectra of **1** in THF-solution following 266 nm excitation for various time delays as indicated in the legend. a) Phenyl mode region. The gray spectrum represents the inverted stationary FTIR spectrum of **1**. b) allene/nitrile stretching region. Numbers indicate peak positions in 1/cm.

oscillation of the $C^5C^{i'}$-distance. Since the N^2C^i bond is more polarized than the $C^5C^{i'}$-bond, the vibrations, ($\mathcal{M}_4$) and ($\mathcal{M}_5$), involving the nitrogen-bound phenyl ring are more intense than the equivalent modes, ($\mathcal{M}_4$)′ and ($\mathcal{M}_5$)′, of the carbon-bound phenyl substituent.

Femtosecond 266 nm-pump/IR-probe spectra recorded in the ring-mode region of **1** in THF solution are reproduced in Figure 4a for a variety of different time delays ranging between 500 fs and 50 ps. Three pronounced negative bands can be detected at exactly the spectral positions of the ($\mathcal{M}_5$), ($\mathcal{M}_5$)′, and ($\mathcal{M}_4$)-modes of the tetrazole. These features represent a pump-induced bleaching of the sample due to the depletion of population in the electronic ground state of **1**. At the same time, two very strong induced absorptions are also detected, which are shifted to lower wavenumbers with respect the ($\mathcal{M}_4$) and ($\mathcal{M}_5$)-bleaching bands. As indicated by the curved arrows in Figure 4, both absorption bands exhibit a pronounced dynamic spectral narrowing and a concomitant delay-dependent shift to higher wavenumbers, which leads to the buildup of two resonances at 1486 cm^{-1} and 1594 cm^{-1}, each having a spectral width that is comparable to that of the bleaching bands. These induced absorptions may arise either from an electronically excited state of **1** or from a photochemical product such as the nitrile imine, **2**.

The (TD)DFT-predicted IR spectrum of the geometry-optimized S_1-state of **1** is displayed in Figure 3 (gray curve, lower panel). It features two induced absorptions, which are indeed shifted to lower wavenumbers relative to the ($\mathcal{M}_4$) and ($\mathcal{M}_5$)-bands of the ground state. However, the frequency-downshift observed in the experiment is much smaller than that predicted by theory. Furthermore, according to the theory, the ($\mathcal{M}_4$) and ($\mathcal{M}_5$)-vibrations of the S_1-state fully delocalize over the entire molecule and thus, couple very strongly to the central five-membered tetrazole ring (see Figure S7. As a result, the excited state absorptions are predicted to be three to ten times as intense as the ground state absorptions. Therefore, neither the spectral positions nor the relative signal strengths of the experimentally observed induced absorptions fully support their assignment to the S_1-state of **1**.

Additional information about the structural evolution of the system can be gleaned from the allene/nitrile stretching region around 2200 cm^{-1}. This is exactly the region in which (hetero)cumulenes and nitrile imines are expected to absorb.[8b,9c] A series of corresponding 266 nm-pump/IR-probe spectra covering delays between 250 fs and 50 ps is displayed in Figure 4b. Much to our surprise, even at the earliest delay, a broad and structureless induced absorption is detected here. It is initially centered around ≈2050 cm^{-1}, but it rapidly shifts within only 1 ps by almost 80 cm^{-1} to higher frequencies while at the same time retaining its structureless profile. Subsequently, the spectral shape of the induced absorption drastically changes. A narrower high-frequency feature centered at ≈2175 cm^{-1} gradually rises and at the same time, a peculiar low-frequency wing reaching all the way out to 2000 cm^{-1} is formed. Finally, on a time scale of several tens of picoseconds, the dominant high-frequency peak progressively shifts to an asymptotic position of 2208 cm^{-1} while its peak height slightly decreases.

Simultaneously, the extended low-frequency wing splits off from the dominant peak and becomes its own distinct spectral feature. As verified by independent step-scan and rapid-scan FTIR-spectroscopy (see Figure S9), the absorption spectrum in the spectral window between 2000 cm^{-1} and 2250 cm^{-1} experiences a common decay following bimolecular kinetics on a time scale of $\approx$100 ms, during which the overall spectral profile is preserved. This strongly suggests that from 50 ps onwards the entire IR-activity in the broad region of Figure 4b is due to a single species only and that this species has a finite lifetime even in the absence of quenchers.

Fitting time-resolved traces at various representative probe wavenumbers with multiexponential kinetics reveals principal components with time constants that fall into the three intervals, (10 ps $\leq \tau_1 \leq$ 20 ps), (2 ps $\leq \tau_2 \leq$ 5 ps), and $\tau_3 \leq$ 0.7 ps (see Figure S10 and Table S3 for fitting results). Thus, according to the UV/IR-data, tetrazole **1** decays upon 266 nm-excitation within the experimental time resolution by cleaving dinitrogen (with a quantum yield of 96 %) and forming a nascent species -presumably a nitrile imine- that exhibits a CN-stretching absorption, which is strongly downshifted with respect to that of a typical organic nitrile. Moreover, it seems as if within several tens of picoseconds, a significant structural relaxation toward the classical nitrile occurs as evidenced by the appearance of the prototypical absorption centered at 2208 cm^{-1}.

However, before such a conclusion can be drawn with confidence, we need to revisit the photochemistry of **1** under cryogenic conditions. Irradiation of **1** in a poly(vinyl chloride) film with 250 nm-light at 85 K was shown to produce nitrile imine **2** (cf. Figure 1c) but with diphenylcarbodiimide, Ph–N=C=N–Ph (**3**) as a side product.[8b] In an Ar-matrix at 12 K, the 254 nm-irradiation also produced **2**, but then a continued irradiation at 370 nm was required for the formation of **3** (cf. Scheme S1 for a survey of the photochemical processes inferred from matrix isolation studies). Importantly, carbodiimide **3** is a heterocumulene and as such, its N=C=N antisymmetric stretching vibration also absorbs in the region of Figure 4b (cf. Figure S11 for the FTIR-spectrum of **3**). To identify conclusively the photochemical product that is responsible for the UV-pump/IR-probe spectrum recorded at the longest delays we improved in a first step the signal-to-noise ratio in the frequency domain by averaging all spectra recorded between 50 ps and 100 ps. Such data processing is allowed because of the shape stability of the spectrum from 50 ps onwards. In addition, we removed the ground-state bleaching bands by subtracting the properly weighted stationary FTIR-spectrum of **1** to obtain a purely absorptive product spectrum that covers both, the region of the phenyl ring modes and the allene/nitrile stretching region.

The result of this analysis is displayed in Figure 5 (upper panel) along with the stationary spectrum of the parent compound. For comparison, the lower panel of Figure 5 displays the DFT-predicted IR-spectra of both the putative nitrile imine product, **2**, and the tetrazole parent, **1**. In the region of the phenyl ring modes, the agreement between experiment and theory is remarkable both, in terms of

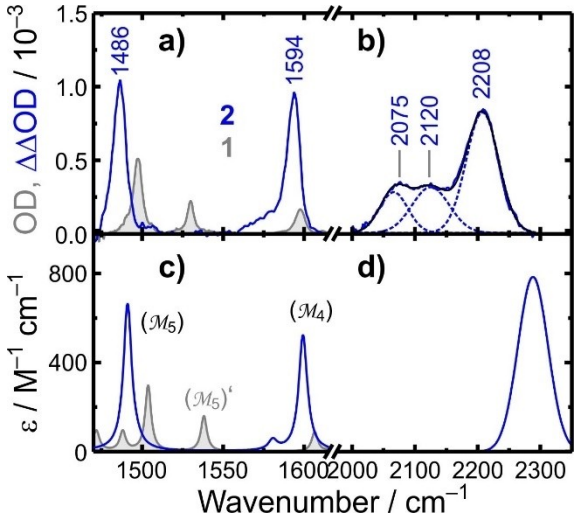

Figure 5. Top panel: Purely absorptive product spectrum obtained upon 266 nm excitation of **1** in THF-solution (blue curve). a) Phenyl mode region. b) Nitrile stretching region. Numbers indicate peak positions in 1/cm. The gray spectra represent the corresponding stationary IR spectrum of **1**. DFT-predicted spectrum of **2** (blue) in comparison with that of **1** (gray) in c) the phenyl mode region and d) the nitrile stretching region.

spectral positions as well as intensities of the product bands with respect to those of the parent. Apart from **2**, the DFT-predicted UV-pump/IR-probe spectra were also computed for other putative stable products including diphenylcarbodiimide, **3**, and those that have been identified previously in matrix isolation studies of the photolysis and thermolysis of mono- and disubstituted tetrazoles.[8b,9c,e] As shown in detail in Figures S11 and S12, none of these products is in reasonable agreement with our UV-pump/IR-probe data in the ring-mode region.

Thus, we can conclude confidently here that the 266 nm-excitation of diphenyltetrazole generates a structurally fully relaxed diphenylnitrile imine after 50 ps. Furthermore, the 1486 cm^{-1} and 1594 cm^{-1} can now be assigned to the ($\mathcal{M}_5$) and ($\mathcal{M}_4$) modes of the phenyl ring attached to the nitrogen terminus of the central nitrile imine moiety of **2** (see also Figures S5 and S8). The conclusion is further corroborated by the previous matrix isolations studies,[9c] which identified these two modes at 1490 cm^{-1} and 1598 cm^{-1} when **2** was trapped in solid argon at 12 K.

In the nitrile stretching region of Figure 5, we notice that averaging has clearly accentuated the fine structure of the absorption band. Apart from the dominant peak at 2208 cm^{-1}, at least two additional maxima at 2075 cm^{-1} and 2120 cm^{-1} can be distinguished. The overall profile can be fitted satisfactorily by a superposition of three Gaussian line shapes (see dashed curves in Figure 5b), which is indicative of the relaxed product, **2**, adopting multiple distinct structures. To reemphasize, the spectral fine structure cannot be assigned to different chemical products because of the spectrally invariant kinetic decay in this window for delays longer than 50 ps. However, from IR-spectra of cryo-trapped nitrile imine species with various substituents, R

and R′, in combinations with DFT calculations, it was concluded that nitrile stretching frequencies above 2150 cm^{-1} are indicative of the R′–CNN–R moiety adopting the propargylic structure (form (i) in Figure 1a) whereas frequencies between 2000 cm^{-1} and 2100 cm^{-1} are signatures of a prevailing heterocumulenic structure (form (ii)).[1c,9c,d]

Thus, we have to conclude here that in THF solution at room temperature, nitrile imine, **2**, adopts several distinct but coexisting structures whose IR-spectroscopic character ranges from propargylic all the way to allenic. These structures can then be regarded as bond-shift isomers on a single adiabatic ground state potential energy surface (PES), and indeed, the monosubstituted nitrile imine, Ph–CNN–H, was recently trapped in a rare gas matrix at 20 K in both, its propargylic and allenic forms at the same time. In the case of **2**, we infer further that at room temperature the system is fully fluxional because of the mutual kinetic decay on the millisecond time scale. These conclusions line up with the notion of nitrile imines being "floppy" molecules.[11a]

As shown in Figure 1c, DFT-calculations clearly favor the propargylic form (i) for **2**. All efforts in identifying a local heterocumulenic minimum energy structure by scanning the singlet PES of ***2*** along the out-of-plane N^2–C^3–$C^{i'}$ angle, α, and the relative twist, θ, between the two phenyl planes were unsuccessful even though a continuum solvation model was invoked (cf. Figure S13 for a contour plot of this relaxed two-dimensional propargylic-to-allenic interconversion potential). Thus, an explicit treatment of the solvent within the framework of an adequate multireference method is probably required to capture correctly a bond shift isomerism of **2** also in terms of theory. It turns out that the relaxed interconversion potential is extremely shallow with an idealized allenic structure ($\alpha = 120°$ and $\theta = 90°$) being energetically only 12 kJ mol^{-1} above the stable propargylic form. This allows the nitrile imine to sample a very wide (α, θ)-configuration space upon thermal excitation at room temperature. A numerical simulation of the spectral profile that takes into account a thermally broadened Boltzmann density in the relaxed interconversion potential is given in the Supporting Information, Figures S14 and S15. Such an analysis demonstrates that the huge spectral width of the IR-activity seen in Figure 5b can indeed be rationalized satisfactorily by the floppy nature of the nitrile imine. However, the model is unable to explain the spectral fine structure, which we attribute to the neglect of discrete solvation.

What remains to be explored is the mechanism leading to elimination of N_2 from **1**. The formation of a thermally and structurally relaxed **2** is observed on a time scale of several tens of picoseconds; yet, the ultrafast appearance of IR-activity around 2050 cm^{-1} (cf. Figure 4b) is very strong evidence that the tetrazole ring has already suffered from the N_2-loss on a sub-picosecond time scale.

At first glance, the extremely rapid nature of the photodissociation seems to be in contradiction with our ability to detect a stationary fluorescence from the solution and the bound nature of the S_1-state as confirmed independently by DFT. Any ultrafast nonradiative deactivation of S_1 will inevitably quench its photoluminescence. The fluorescence quantum yield is normally given by $\Phi_f = k_r/(k_{nr} + k_r)$, where k_r is the radiative rate and k_{nr} is the rate constant for the nonradiative deactivation channel; that is, an internal conversion, an intersystem crossing (ISC), or a photochemical conversion such as the N_2-loss. This however immediately suggests that N_2 cannot be eliminated from the locally excited singlet π–π* state. Rather, N_2 must be eliminated from a lower-lying excited state, which in the case of **1** can only be a triplet state (see the above discussion regarding the electronic structure of **1** and Figure S6). Interestingly, the 0–0 transition can be located from the stationary absorption and emission spectra in Figure 1a at a wavelength of 303 nm. Thus, a 266 nm-photon prepares S_1 with excess vibrational energy of roughly 55 kJ mol^{-1}. If intersystem crossing necessitates this excess energy, it must compete with the inevitable dynamics of vibrational energy relaxation (VER). The initial processes can then be written succinctly (cf. Scheme 1) as a branched decay of the optically prepared hot π–π* state, S_1^{hot}, either into the triplet manifold, ^{3}**1** (T_n), which ultimately leads to N_2-elimination and nitrile imine formation, or into the relaxed π–π* state, S_1^{rel}, whose only decay path is photoluminescence.

In this notion, the fluorescence quantum yield equals the quantum yield for the formation of S_1^{rel}, i.e. $\Phi_f = k_{VER}/(k_{ISC} + k_{VER})$. Using the inverse of the appearance time of the induced absorption at 2050 cm^{-1} as a lower limit for the intersystem crossing rate, i.e. $k_{ISC} = 1/0.25$ ps, and neglecting any other deactivation channels for S_1^{rel}, a perfectly reasonable vibrational relaxation rate of $k_{VER} = 1/6$ ps would bring the experimentally observed fluorescence quantum yield in harmony with the ultrafast photodissociation; i.e. $\Phi_f = 0.04$. Thus, Scheme 1 is able to reconcile the two seemingly contradictory observations (ultrafast nitrile imine formation on the one hand and sizeable stationary fluorescence on the other) with perfectly realistic rate parameters.

To test these notions in greater detail relaxed PES scans were conducted along the distance between the centroids of the two fragments, X=N^3–N^4 and Y=C^5–N^1–N^2, and along the two local bond lengths, $r(N^2–N^3)$ and $r(C^5–N^4)$ (see Figure 6a). The former scan represents the concerted breakage of the two bonds, C^5–N^4 and N^2–N^3, while the latter tracks the stepwise bond breakage via the ring-opened intermediate, Ph–$C^5(N_2)$–N^1=N^2–Ph, i.e. (*E*)-1-(diazo-(phenyl)methyl)-2-phenyldiazene, (**4**, cf. Figure 6b and Scheme S1). On the relaxed S_0-surface (gray potential), species **4** corresponds to a shallow minimum with an energy of 172 kJ mol^{-1} relative to **1** and the succeeding elimination process, **4**→**2** + N_2, necessitates the crossing of a barrier of 56 kJ mol^{-1}. In contrast, the barrier along the X–Y intercentroid distance amounts to only 210 kJ mol^{-1}. These

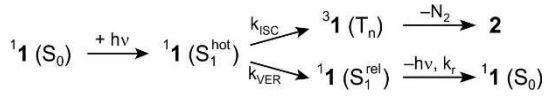

Scheme 1. Excited-state decay competition between vibrational energy relaxation leading to photoluminescence and intersystem crossing leading to nitrile imine formation.

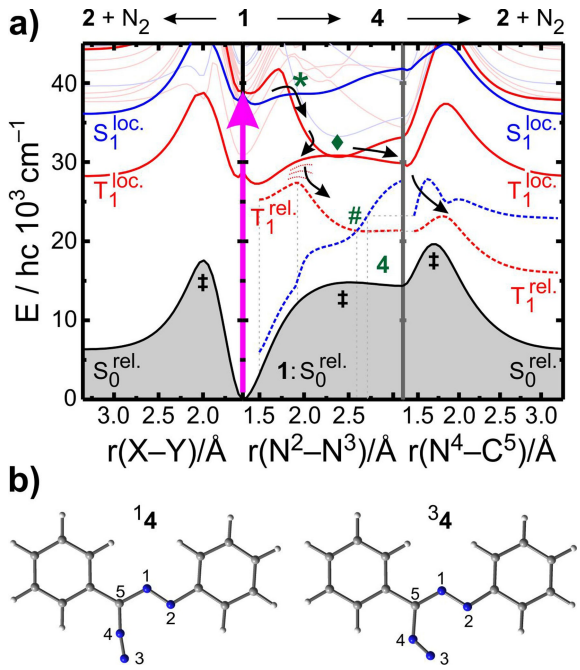

Figure 6. a) Potential energy surfaces along the reaction coordinates for the concerted (**1**→**2**+N_2) and the stepwise (**1**→**4**→**2**+N_2) 1,3-dipolar cycloelimination, The gray surface is the relaxed adiabatic S_0-surface. Solid curves represent the corresponding local singlet (blue) and triplet (red) PESs. The dashed red curve represents the relaxed adiabatic T_1-surface and the dashed blue curve is its corresponding local S_0-surface. The asterisk and hash mark indicate singlet–triplet, the diamond triplet–triplet curve crossings, and the daggers indicate energy barriers. The short-dashed curves represent an out-of-plane structural relaxation of the T_1-state. b) DFT-optimized structure of singlet and triplet (*E*)-1-(diazo(phenyl)methyl)-2-phenyldiazene. Left: ^{1}**4** is fully planar. Right: ^{3}**4** is non-planar.

numbers suggest that the concerted mechanism of the thermal 1,3-dipolar cycloelimination of N_2 from **1** is slightly favored over the stepwise mechanism.

The UV-absorption, however, initiates the same elimination from the locally excited S_1-state of **1** (blue curve, Figure 6a). Motion along the N^2–N^3 distance away from the Franck–Condon region brings the system to an energetically lower-lying curve crossing (marked by an asterisk) with a higher triplet state, which in turn exhibits a steep gradient towards a geometry resembling **4** (indicated by a diamond). Here, the system can reach the triplet ground state via internal conversion. A very small out-of-plane distortion suffices to relax the T_1-state energetically. The minimum energy structure on the adiabatic T_1-surface is indeed a ring-opened diradical form as shown in Figure 6b. However, even when energetically relaxed, ^{3}**4** is also a highly unstable species because i) it matches nearly perfectly a geometry, at which the T_1^{rel}- and S_0-surfaces cross (hash mark in Figure 6a), and ii) it is energetically located above the ground-state barriers for N_2-loss.

According to these calculations, the N_2-loss is effectively facilitated by a sequence of ultrafast non-adiabatic transitions that shuttle the system from the singlet to the triplet and back to the singlet manifold without requiring any large-amplitude structural modifications except for motion along the N^2–N^3 displacement. These initial stages preconfigure the system in both, its electronic and nuclear degrees of freedom for the final cleavage of the N^4–C^5 bond with generation of dinitrogen and **2** in its singlet electronic ground state.

Importantly, once the system has crossed either of the two higher S_0-barriers, the nascent product emerges with a bent CNN-moiety that reminds us of the carbenic, the two dipolar, and the diradical forms of nitrile imines as depicted in Figure 1a. Therefore, at the barrier top, the system has not yet acquired the full C≡N triple-bond character of the propargylic form or the C=N=N heterocumulenic character of the allenic form of a nitrile imine. The final motion towards the asymptotic limits of Figure 6a affect the relative orientation of the two phenyl rings and will therefore be hindered by solvent friction. Hence, we can envision the evolution from the barrier top toward the well-separated fragments, **2**+N_2, as a creeping motion along the bottom of the adiabatic S_0-PES; a motion, which takes place on a time scale of up to tens of picoseconds during which the system will gradually acquire its full nitrile/cumulenic stretching vibrational character. We can follow this biphasic evolution of the system IR-spectroscopically most clearly in the C≡N/C=N=N stretching region: The initial electronic relaxation and the ring-opening dynamics manifest themselves in an ultrarapid (within the time-resolution) appearance of the broad and structureless band at the very low-frequency edge of Figure 4b. The ensuing loss of the dinitrogen fragment and the downhill creeping motion on the adiabatic S_0-surface from the barrier top toward the fully relaxed products is then reflected in the continuous frequency-upshift of this absorption and the emergence of the peculiar spectral fine structure on a tens of picoseconds scale.

Conclusion

In summary, we have been able to disclose the elementary dynamics of the photoinduced 1,3-dipolar cycloelimination of dinitrogen from the model system, 2,5-diphenyltetrazole, and the concomitant formation of the elusive nitrile imine using the structure-sensitive technique of femtosecond UV-pump/IR-probe spectroscopy. Aided by detailed DFT and TDDFT calculations, we could sketch a molecular-level mechanism that is compatible with the complex IR-spectro-temporal evolution in the phenyl ring mode region and the nitrile/allene stretching region. Specifically, we found that N_2 is cleaved from the tetrazole within less than 500 fs in a consecutive rather than a concerted fashion and N_2-loss is brought about by a sequence of non-adiabatic transitions. The intermediate singlet diazodiazene structure is energetically located above the barrier for N^4–C^5 bond breakage and can thus not be observed. However, the departing N_2-molecule leaves behind a nitrile imine fragment that is strongly distorted along its CNN-angle, and thus reminiscent of the carbonic, dipolar, and diradical forms rather than the allenic or propargylic forms that are normally adopted by nitrile imines. At early times (<500 fs), the IR-absorption in

the allene/nitrile stretching region reports on the evolution of the system toward the favored propargylic form while its spectral profile at late delays (>50 ps) attests the final product a high degree of structural flexibility. The fully relaxed nitrile imine is elusive in nature, it has a lifetime of ≈100 ms under the photochemical conditions of our experiments, and it decays in the absence of substrates presumably by dimerization according to second-order kinetics. We are currently engaged in quenching experiments of nitrile imines that are aimed at exploring the chemical reactivity of these intriguing species in more detail. Finally, we emphasize that a proper theoretical treatment of the molecular dynamics leading to the formation of nitrile imines by N_2-elimination from tetrazoles requires theoretical models that are far more sophisticated than those we have applied herein. Ab initio molecular dynamics simulations are urgently needed that take into account the multireference character of nitrile imines properly and include a realistic explicit solvation approach.

Acknowledgements

Financial support by the Deutsche Forschungsgemeinschaft is gratefully acknowledged. S.F. thanks the Fond der chemischen Industrie for granting a dissertation stipend. Open Access funding enabled and organized by Projekt DEAL.

Conflict of Interest

The authors declare no conflict of interest.

Data Availability Statement

The data that support the findings of this study are available from the corresponding author upon reasonable request.

Keywords: 1,3-Dipolar Cycloaddition · Femtochemistry · Infrared Spectroscopy · Photodissociation · Reactive Intermediates

[1] a) C. Jamieson, K. Livingstone, *Properties, Reactivity and Applications*, Springer Nature Switzerland, Cham, **2020**; b) R. Huisgen, M. Seidel, J. Sauer, J. W. McFarland, G. Wallbillich, *J. Org. Chem.* **1959**, *24*, 892–893; c) G. Bertrand, C. Wentrup, *Angew. Chem. Int. Ed. Engl.* **1994**, *33*, 527–545; *Angew. Chem.* **1994**, *106*, 549–568.

[2] R. Huisgen, *Angew. Chem. Int. Ed. Engl.* **1963**, *2*, 633–645; *Angew. Chem.* **1963**, *75*, 742–754.

[3] J. T. Sharp in *Synthetic Applications of 1,3-Dipolar Cycloaddition Chemistry Toward Heterocycles and Natural Products* (Eds.: A. Padwa, W. H. Pearson), Wiley, Ney York, **2002**, pp. 473–537.

[4] R. Darkow, M. Yoshikawa, T. Kitao, G. Tomaschewski, J. Schellenberg, *J. Polym. Sci. Part A* **1994**, *32*, 1657–1664.

[5] J. K. Stille, A. T. Chen, *Macromolecules* **1972**, *5*, 377–384.

[6] C. Rodriguez-Emmenegger, C. M. Preuss, B. Yameen, O. Pop-Georgievski, M. Bachmann, J. O. Mueller, M. Bruns, A. S. Goldmann, M. Bastmeyer, C. Barner-Kowollik, *Adv. Mater.* **2013**, *25*, 6123–6127.

[7] Z. Li, L. Qian, L. Li, J. C. Bernhammer, H. V. Huynh, J.-S. Lee, S. Q. Yao, *Angew. Chem. Int. Ed.* **2016**, *55*, 2002–2006; *Angew. Chem.* **2016**, *128*, 2042–2046.

[8] a) W. Sieber, P. Gilgen, S. Chaloupka, H.-J. Hansen, H. Schmid, *Helv. Chim. Acta* **1973**, *56*, 1679–1690; b) N. H. Toubro, A. Holm, *J. Am. Chem. Soc.* **1980**, *102*, 2093–2094; c) C. Wentrup, R. Flammang, *J. Phys. Org. Chem.* **1998**, *11*, 350–355.

[9] a) G. Maier, J. Eckwert, A. Bothur, H. P. Reisenauer, C. Schmidt, *Liebigs Ann.* **1996**, 1041–1053; b) B. Braida, C. Walter, B. Engels, P. C. Hiberty, *J. Am. Chem. Soc.* **2010**, *132*, 7631–7637; c) D. Bégué, G. G. Qiao, C. Wentrup, *J. Am. Chem. Soc.* **2012**, *134*, 5339–5350; d) D. Bégué, C. Wentrup, *J. Org. Chem.* **2014**, *79*, 1418–1426; e) C. M. Nunes, I. Reva, R. Fausto, D. Bégué, C. Wentrup, *Chem. Commun.* **2015**, *51*, 14712–14715; f) C. M. Nunes, I. Reva, M. T. S. Rosado, R. Fausto, *Eur. J. Org. Chem.* **2015**, 7484–7493.

[10] a) M. W. Wong, C. Wentrup, *J. Am. Chem. Soc.* **1993**, *115*, 7743–7746; b) F. Cargnoni, G. Molteni, D. L. Cooper, M. Raimondi, A. Ponti, *Chem. Commun.* **2006**, 1030–1032; c) H. M. Muchall, *J. Phys. Chem. A* **2011**, *115*, 13694–13705; d) M. M. Montero-Campillo, I. Alkorta, J. Elguero, *Sci. Rep.* **2017**, *7*, 6115; e) P. C. Hiberty, G. Ohanessian, *J. Am. Chem. Soc.* **1982**, *104*, 66–70; f) R. C. Mawhinney, H. M. Muchall, G. H. Peslherbe, *Chem. Commun.* **2004**, 1862–1863.

[11] a) P. Caramella, K. N. Houk, *J. Am. Chem. Soc.* **1976**, *98*, 6397–6399; b) J.-L. Fauré, R. Réau, M. W. Wong, R. Koch, C. Wentrup, G. Bertrand, *J. Am. Chem. Soc.* **1997**, *119*, 2819–2824.

[12] G. da Silva, J. W. Bozzelli, *J. Org. Chem.* **2008**, *73*, 1343–1353.

[13] K. Bhattacharyya, D. Ramaiah, P. K. Das, M. V. George, *J. Photochem.* **1987**, *36*, 63–84.

[14] P. Vöhringer, *Dalton Trans.* **2020**, *49*, 256–266.

[15] R. L. Martin, *J. Chem. Phys.* **2003**, *118*, 4775–4777.

[16] M. A. F. de Souza, E. Ventura, R. C. M. U. Araújo, M. N. Ramos, S. A. do Monte, *J. Comput. Chem.* **2009**, *30*, 1075–1081.

[17] A. M. Gardner, T. G. Wright, *J. Chem. Phys.* **2011**, *135*, 114305.

Manuscript received: April 20, 2022
Accepted manuscript online: May 18, 2022
Version of record online: June 7, 2022